

Heating of the solar atmosphere by strong damping of Alfvén waves

P. Song¹ and V. M. Vasyliūnas^{1,2}

Received 22 March 2011; revised 24 May 2011; accepted 28 June 2011; published 27 September 2011.

[1] The heating of the solar atmosphere by strongly damped Alfvén waves that produce heating through plasma-neutral collisions is studied by solving analytically a self-consistent one-dimensional model of the plasma-neutral-electromagnetic system. We compute the vertical profile of the wave spectrum and power by a novel method, which includes the damping effect neglected in previous treatments, and find that the damping depends on the magnetic field strength. The damping is extremely strong for weaker magnetic field and less strong for strong field. Under either condition, the high-frequency portion of the source power spectrum is strongly damped at the lower altitudes, depositing heat there, whereas the lower-frequency perturbations are nearly undamped and can be observed in the corona and above when the field is strong. The chromosphere behaves like a low-pass filter. The magnetic field strength determines the upper cutoff frequency. As a result, the power and spectrum of the waves observed above the corona is weak for regions of weaker background magnetic field and only a fraction of those at the photosphere for regions of strong magnetic field. Contrary to what was supposed in some earlier Alfvén wave damping models, the spectrum observed above the chromosphere in general does not represent the energy input. We show, using the parameters of a semi-empirical model for quiet-Sun conditions, that this mechanism, without invoking any anomalous processes, can generate sufficient heat to account for the radiative losses in the atmosphere, with most of the heat deposited as required at lower altitudes.

Citation: Song, P., and V. M. Vasyliūnas (2011), Heating of the solar atmosphere by strong damping of Alfvén waves, *J. Geophys. Res.*, 116, A09104, doi:10.1029/2011JA016679.

1. Introduction

[2] The thermal structure of the atmosphere of the Sun and other solar-type stars has been one of the outstanding problems in solar physics and astrophysics for decades [e.g., *Van de Hulst*, 1953; *Parker*, 1965, 1991; *Athay*, 1976; *Withbroe and Noyes*, 1977; *Böhm-Vitense*, 1984; *Hollweg*, 1985, 1986; *Narain and Ulmschneider*, 1990, 1996; *Priest*, 2000; *Ulmschneider*, 2001; *Aschwanden*, 2005; *Fossum and Carlsson*, 2005; *Cranmer et al.*, 2007]. Above the surface of the star, powerful heating processes must be occurring to supply the energy lost by radiation and at the same time to raise the temperature by a large factor; in the case of the Sun (see Figure 1a), the temperature increases from ~6000 degrees in the chromosphere (not much different from that in the photosphere) to ~2 million degrees in the corona. Associated with the heating, massive ionization of the neutral atmosphere of a solar-type star takes place: the corona is

nearly fully ionized, while below the transition region in the chromosphere the gases are weakly ionized at lower altitude and partially ionized at higher altitude (see Figure 1a).

[3] Although this heating of the solar atmosphere is often referred to by the single generic name of coronal heating, two distinct aspects of the problem with rather different physical requirements can be recognized. The first is to explain how the high temperatures are reached; the second is to account for the energy supply. In the corona, the primary question is what process can raise the temperature to values that exceed by far anything expected from simple thermodynamic considerations; the amount of energy involved, given the low mass densities, however, is relatively small. In the chromosphere, by contrast, the temperatures values are not particularly out of the ordinary, but the main question is to identify the energy supply which, in order to balance the radiative losses, is here required to be more than an order of magnitude larger than in the corona.

[4] In this paper we concentrate on the second aspect. As a starting point, we focus on quiet conditions and leave more complicated situations for future studies. For the quiet Sun, most of the energy is lost in the lower and middle chromosphere and the energy losses in all higher regions (including the corona) are smaller by an order of magnitude or more. The principal challenge, therefore, of the solar

¹Center for Atmospheric Research and Department of Environmental, Earth and Atmospheric Sciences, University of Massachusetts Lowell, Lowell, Massachusetts, USA.

²Max-Planck-Institut für Sonnensystemforschung, Katlenburg-Lindau, Germany.

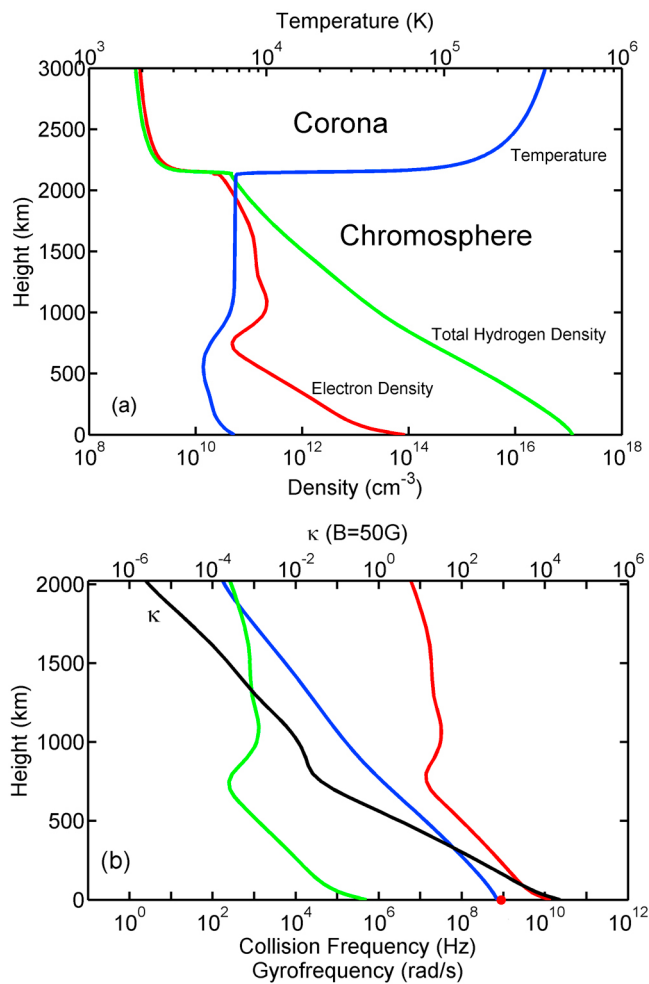


Figure 1. (a) Temperature (blue line), total hydrogen number density (green line) and electron number density (red line) [Avrett and Loeser, 2008]. (b) Electron collision frequency $\nu_e = \nu_{ei} + \nu_{en}$ (red line), ion-neutral collision frequency ν_{in} (blue line), neutral-ion collision frequency ν_{ni} (green line), and ratio of collision frequencies to gyrofrequencies, parameter $\kappa = \nu_e \nu_i / \Omega_e \Omega_i$ for $B = 50\text{G}$ (black line), all calculated from the formulas of De Pontieu *et al.* [2001] and the parameters of Avrett and Loeser [2008]. The electron gyrofrequency Ω_e for $B = 50\text{G}$ is indicated as a solid red dot on the x axis.

atmosphere heating problem is to explain the heating mechanisms in the lower and middle chromosphere.

[5] In the optically thin region above the photosphere, the temperature profile is maintained locally by the heating process (i.e., conversion into heat of other forms of energy) and the radiative losses as well as remotely by the conductive heat flux and the advective energy transfer. If the temperature gradient is small, heat conduction and energy advection are relatively unimportant, and a local heating process has to balance the energy loss by radiation. Table 1, adapted from Withbroe and Noyes [1977], summarizes the empirical estimates of the energy loss rates per unit area (i.e., integrated over altitude) for various regions. The local heating rate required to balance the radiation loss is estimated to be $10^{-1} \text{ erg cm}^{-3} \text{ s}^{-1}$ in the lower and $10^{-2} \text{ erg cm}^{-3} \text{ s}^{-1}$ in the

higher chromosphere [Vernazza *et al.*, 1981]. Integrated over 2000 km altitude range where the temperature varies relatively slowly, this gives a total power of $10^{6-7} \text{ erg cm}^{-2} \text{ s}^{-1}$, depending on solar activity and specific location on the Sun, in general agreement with the results of Withbroe and Noyes [1977]. By comparison (see Table 1), the power input to the corona is smaller by roughly an order of magnitude, and the power required to maintain the solar wind (a form of advective energy transfer) is smaller by one more order of magnitude, representing only a small fraction of the power going into the radiative loss.

[6] Although many models and mechanisms have been proposed [see Hollweg, 1985; Narain and Ulmschneider, 1990, 1996; Aschwanden, 2005; Cranmer *et al.*, 2007], their heat conversion efficiencies are generally inadequate to supply the radiative heat loss from the observed available power. Furthermore, most proposed heating mechanisms are efficient only at the higher altitudes, i.e., above 800 km, whereas, as noted above, heat energy is lost by radiation predominantly at the lower altitudes. It is commonly assumed that the power must be supplied from below the photosphere, probably as upward flux of energy in some form of low frequency waves or turbulence. The upper limit on the kinetic energy associated with the thermal perturbations is $\rho_t V_{th}^2 / 2 \sim 10^3 \text{ erg/cm}^3$, where ρ_t ($\sim 2.8 \times 10^{-7} \text{ g/cm}^3$) and V_{th} ($\sim 10 \text{ km/s}$), are the total mass density and the mean thermal speed, respectively, of the fluid at the surface of the photosphere. According to a semi-empirical model [Avrett and Loeser, 2008], the average perturbation velocity is about 1.7 km/s, well below V_{th} ; this corresponds to a kinetic energy density of $4 \times 10^3 \text{ erg/cm}^3$ for motion in one dimension. If the perturbations are isotropic, the energy flux density (energy density multiplied by the propagation velocity) upward from the photosphere is $4 \times 10^9 \text{ erg cm}^{-2} \text{ s}^{-1}$ for acoustic waves (vertical oscillation). For Alfvén waves (horizontal oscillations in two dimensions), if propagating at the total Alfvén speed as discussed later, the energy flux is $4 \times 10^8 \text{ erg cm}^{-2} \text{ s}^{-1}$ for a background magnetic field of 1 Gauss and $4 \times 10^9 \text{ erg cm}^{-2} \text{ s}^{-1}$ for 10 Gauss. The energy flux for Alfvén waves is correspondingly greater (for a given amplitude of the velocity perturbation) in regions of stronger magnetic fields.

[7] Evidently, either wave mode can in principle provide an energy supply adequate for heating to sustain the radiation [Erdélyi and Fedun, 2007], not to mention the small amount needed to launch the solar wind. The problem is thus not the source of the energy as such but the question, what mechanism can efficiently convert the wave energy into thermal energy in the atmosphere, while maintaining the observational constraints that the heating must be stronger in the lower chromosphere [e.g., Aschwanden, 2005] where a larger fraction of the radiation is emitted, and that the wave power leaking into the corona must not exceed the wave power observed there, which is only of the order of $10^6 \text{ erg cm}^{-2} \text{ s}^{-1}$ [Narain and Ulmschneider, 1990].

[8] Wave heating mechanisms have been proposed [see Narain and Ulmschneider, 1990], in which heating can be driven by basically two types of flow perturbations: (compressional) longitudinal and (incompressible) transverse or torsional. Acoustic modes, often investigated separately, are a limiting case of compressional magnetohydrodynamic modes with negligible magnetic field. Although the power

Table 1. Chromospheric and Coronal Energy Losses^a

Parameter	Quiet Sun	Coronal Hole	Active Region
Transition layer pressure (dyn cm ⁻²)	2×10^{-1}	7×10^{-2}	2
Coronal temperature (K, at $r \approx 1.1R_{\odot}$)	1.1 to 1.6×10^6	10^6	2.5×10^6
<i>Coronal Energy Losses per Unit Area (erg cm⁻² sec⁻¹)</i>			
Conduction flux F_c	2×10^5	6×10^4	10^5 to 10^7
Radiative flux F_r	10^5	10^4	5×10^6
Solar wind flux F_w	$\lesssim 5 \times 10^4$	7×10^5	(< 10^5)
Total corona loss $F_c + F_r + F_w$	3×10^5	8×10^5	10^7
<i>Chromospheric Radiative Losses per Unit Area (erg cm⁻² sec⁻¹)^b</i>			
Lower chromosphere	2×10^6	2×10^6	$\gtrsim 10^7$
Middle chromosphere	2×10^6	2×10^6	10^7
Upper chromosphere	3×10^5	3×10^5	2×10^6
Total chromospheric loss	4×10^6	4×10^6	2×10^7
Solar wind mass loss (g cm ⁻² sec ⁻¹)	$\lesssim 2 \times 10^{-11}$	2×10^{-10}	(< 4×10^{-11})

^aFrom *Withbroe and Noyes* [1977] (reproduced with permission of *Annual Review of Astronomy and Astrophysics*; permission conveyed through Copyright Clearance Center, Inc.).

^bBased on estimates for the quiet Sun by *Athay* [1976].

available for incompressible modes is probably much greater (by a factor ~ 30) than that available for compressional modes [*Ulmschneider*, 2001; *Jess et al.*, 2009], the latter (in particular the acoustic modes) have nonetheless been mostly favored as heating mechanisms by theorists, perhaps because as they propagate upward the perturbation amplitude can easily increase with altitude (for a fixed energy flux), leading to wave steepening and the consequent formation of shocks which are efficient converters of flow kinetic energy into thermal energy; note, however, that this shock heating may be effective only at the higher altitudes where wave steepening occurs, not in the lower chromosphere where most heating is required.

[9] Except perhaps for limited effects of turbulence, it is difficult to obtain significant heating from incompressible modes in the acoustic (negligible-magnetic field) limit, in which, furthermore, horizontal (transverse or torsional) flow perturbations do not propagate from low to higher altitude. Transverse incompressible modes become important when there is a magnetic field, particularly one that has a vertical component; perturbations propagating upward from the photosphere can be described by Alfvén waves, their amplitude increasing with height [e.g., *Banerjee et al.*, 2009]. The transverse modes may, through various damping mechanisms, play an important role in heating the corona where the magnetic field is strong and the medium nearly fully ionized [e.g., *Parker*, 1965; *Hollweg and Isenberg*, 2002]. In the chromosphere, however, on the basis of previous theories, the observed chromospheric Alfvén waves may provide heating around 10^5 erg cm⁻² s⁻¹ [*De Pontieu et al.*, 2007], comparable to the power into the solar wind but an order or more of magnitude smaller than the radiation loss from the chromosphere [*Withbroe and Noyes*, 1977]. This discrepancy may indicate that the mechanism of heating by Alfvén waves is deficient, or it may mean that previously applied theories are flawed.

[10] Most recently, mechanisms that include the coupling between the vertical and horizontal perturbations have been

proposed [e.g., *Van Doorsselaere et al.*, 2008; *Terradas et al.*, 2010; *Verth et al.*, 2010; *Soler et al.*, 2011; *Vasheghani Farahani et al.*, 2011]. Most of these theories have focused on coronal applications and, to our knowledge, have not been able to predict the required chromospheric heating rate.

[11] In this study we seek to explain chromospheric heating by identifying a mechanism that can efficiently convert available wave power into heat at the required places and in the required amounts. We focus on properties of the chromosphere as a partially ionized medium, invoking the counterpart of transverse Alfvén waves in such a medium. We describe qualitatively the essential physical ideas of the proposed mechanism in section 2, develop a simple analytical model in section 3, and apply its results to the solar chromosphere in section 4, with discussion in section 5 and conclusions in section 6.

2. The Mechanism: Physical Description

2.1. Overview and Assumptions

[12] We propose that solar atmospheric heating is driven by transverse or torsional, i.e., horizontal, oscillatory bulk flows of plasma below the photosphere and takes place through the collisions between the plasma and the neutral gas. The essence of the process is that, because the chromosphere is only partially (and over much of its volume very weakly) ionized, the plasma and the neutral atmosphere can be treated as two distinct fluids, subject to different forces and therefore possibly moving differently; the systematic difference in bulk velocity may be small but, if maintained permanently through imposed oscillations, may produce considerable energy dissipation (heating) by inter-species collisions of the two media. Such a process has been proposed previously and investigated under the rubric of damping Alfvén wave models [*Piddington*, 1956; *Osterbrock*, 1961; *Haerendel*, 1992; *De Pontieu et al.*, 2001; *Goodman*, 2004; *Khodachenko et al.*, 2004; *Leake et al.*, 2005]. Early models treated the system as a single fluid and the Alfvén waves as weakly damped, with the wave amplitude and spectrum not changing significantly with altitude (essentially the same assumption as the well-known Born approximation of scattering theory). The problem with this approach is that the energy appearing as heat is the energy taken out of the wave by damping; hence weak damping means weak heating, and it is no surprise that the heating rates derived from these earlier models are insufficient to heat the solar atmosphere. *De Pontieu et al.* [2001] and *Leake et al.* [2005] did note that the damping may be heavy at high frequencies; however, *De Pontieu et al.*'s treatment was still based on the Born approximation and hence not applicable to strongly damped waves, while *Leake et al.* did not calculate a heating rate.

[13] The critical issue is thus how to treat a system with strong damping. The new aspects in the present study are: (a) we allow from the outset for the possibility of strong damping or even complete absorption of waves, depending on wave frequency and background magnetic field strength; (b) we calculate the heating rate directly and from it determine self-consistently the altitude variation of wave amplitudes, by a simple general method which does not require detailed solution of wave equations in an inhomogeneous

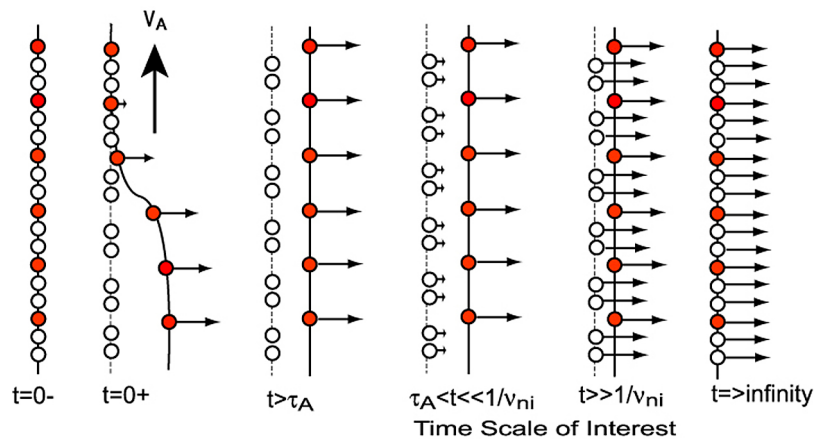


Figure 2. Electromagnetic coupling in a partially ionized fluid. Red dots indicate ions and open circles indicate neutrals. Sketch of plasma and neutral motion in a stratified one-dimensional situation with a vertical magnetic field, after a horizontal flow of plasma and neutrals has been imposed below the lower boundary, starting at $t = 0$. With its vertical extent taken as $L = V_A T_A \ll V_A / \nu_{ni}$, the figure represents only a localized small segment of the entire system.

medium; (c) we assume a broad frequency spectrum of waves at the source and exploit the increased heating efficiency at higher frequencies and as a function of the background magnetic field. As a result, we predict (for the first time, to our knowledge) a vertical profile of heating in the chromosphere that is concentrated toward low altitudes, as required by the observations, and a heating rate (computed without invoking any “anomalous” process) that is sufficient to account for the observed radiative losses, given a reasonable input wave power from the photosphere.

2.2. The Alfvén Wave in a Partially Ionized Medium

[14] It may be illuminating, before plunging into the equations, to consider a qualitative picture of how an Alfvén wave propagates in a fluid consisting of plasma and neutrals. Figure 2 illustrates the process in a simple locally 1-dimensional stratified solar atmosphere with a vertical magnetic field. We consider purely horizontal bulk motions, so gravity (which acts on all the particles) may be ignored. Electromagnetic forces act only on the plasma, not on the neutrals. Plasma and neutrals interact only through collisions; neutrals are affected by the plasma on the time scale $1/\nu_{ni}$, the reciprocal of the neutral-ion collision frequency.

[15] Now impose at the lower boundary a horizontal flow of both plasma and neutrals, as a very short small step increase at time $t = 0+$. The neutrals above the boundary are initially unaffected (at least insofar as viscosity can be neglected) and remain at rest. The moving plasma, however, because the magnetic field is frozen to it, immediately creates a magnetic field line kink at the boundary, which exerts a tension force on the plasma above and makes it flow, creating another kink higher up, and so on. The net result is a magnetic perturbation front propagating upward along the magnetic field at the Alfvén speed, with the plasma behind the front flowing horizontally. As long as the elapsed time since $t = 0$ is short compared to $1/\nu_{in}$, where $1/\nu_{in}$ is the ion-neutral collision period, the plasma is essentially unaffected by the neutrals and the Alfvén speed, $V_A = B/(\mu_0 \rho_i)^{1/2}$, is that derived from the magnitude B of the magnetic field and

from the mass density ρ_i of the plasma only. The velocity difference between the plasma and the neutrals, however, leads to momentum transfer by collisions between the two species which accelerate the neutrals, increasing their flow speed from zero at $t = 0$ up to almost the same speed as the plasma after an elapsed time of order $1/\nu_{ni}$. The collisions tend also to slow down the plasma, but its original speed is maintained all this time by the continued imposed flow at the lower boundary, through the tension force of a magnetic field line kink propagating upward as before but now, in the time interval from approximately $1/\nu_{in}$ to well after $1/\nu_{ni}$, at the (much slower) Alfvén speed derived from the total mass density ρ_t of the entire medium (plasma plus neutrals). The horizontal velocity difference between neutral and plasma flow decreases steadily at exponential time scale $1/\nu_{ni}$, until eventually, as the elapsed time goes to infinity, the plasma and neutrals reach the final asymptotic state when the two species move at a common speed, equal to that imposed at the lower boundary.

[16] This sequence, depicted in Figure 2, goes from an initial state of rest, through a transient phase of plasma-neutral flow difference, to a final state of equal plasma-neutral flow, all a consequence of an Alfvén wave launched by imposing a small velocity step at the boundary. A small step function can be decomposed into a spectrum of plane waves, which (since Alfvén waves are nondispersive) propagate all at the same speed, hence the shape of the initial perturbation does not change. Now any time profile of perturbations at the lower boundary can be built up as a series of such small steps, including oscillations (for which the true asymptotic steady state of no flow difference is never reached). If the perturbations continue without end but always vary more slowly than the neutral-plasma collision time, the system remains in a slowly varying quasi-steady state, with a small but nonzero velocity difference between plasma and neutrals and consequent heating by collisions. The focus of our mathematical development is on this regime.

[17] The above 1-dimensional description is highly simplified. In general, there will also be compressible modes

generated by horizontal nonuniformities, as well as by a horizontally propagating component when the magnetic field is at an angle to the vertical.

[18] Conventional description of heating by damping of Alfvén waves, in contrast, has treated the plasma and neutrals as a single fluid in which the Alfvén waves propagate, with dissipation arising by Ohmic or Joule heating within the medium. This over-simplified description masks the physical processes that take place in the system and may be conceptually misleading. Contrary to the common assumption of a purely Ohmic or Joule heating, *Vasyliūnas and Song* [2005] have pointed out that the dissipative heating in a collisional partially ionized flow contains two contributions: the frictional heating, by ion-neutral collisions from the relative flow, and the Ohmic or Joule heating proper, by electron collisions from the current. In both mechanisms, the heating results ultimately from the velocity difference between the plasma and neutrals, hence more heat is produced when the velocity difference is greater. For oscillatory perturbations, the velocity difference increases with increasing frequency; higher frequency perturbations thus produce more heat (and also are subject to heavier damping) than lower frequency ones. In addition, since the true Ohmic heating results from electron collisions, less heat is produced in strong magnetic fields, in which electron gyromotion is more dominant relative to collision effects.

3. The Model: Analytic Treatment of a Stratified Atmosphere

3.1. Basic Equations and Approximations

[19] We now treat analytically a system consisting of plasma, neutral medium, and electromagnetic fields, geometrically simplified but self-consistent in all three constituents. The momentum equations for the electrons, ions, and neutrals can be combined and rewritten [*Song et al.*, 2005, 2009; *Vasyliūnas and Song*, 2005] as the generalized Ohm's law, the plasma momentum equation and the neutral momentum equation, the leading terms of which are:

$$0 = N_e e (\mathbf{E} + \mathbf{V} \times \mathbf{B}) - \mathbf{j} \times \mathbf{B} - \frac{m_e}{e} (\nu_{ei} + \nu_{en}) \mathbf{j}, \quad (1)$$

$$\rho_i \frac{\partial \mathbf{V}}{\partial t} = \mathbf{j} \times \mathbf{B} - \rho_i \nu_{in} (\mathbf{V} - \mathbf{U}), \quad (2)$$

and

$$\rho_n \frac{\partial \mathbf{U}}{\partial t} = \rho_n \nu_{ni} (\mathbf{V} - \mathbf{U}), \quad (3)$$

where e , ρ_η , \mathbf{j} , \mathbf{V} , \mathbf{U} , \mathbf{E} , \mathbf{B} , N_e , and $\nu_{\eta\xi}$ are the elementary electric charge, the mass density of species η , the electric current, the bulk velocities of the plasma and neutrals, the electric and the magnetic fields, electron concentration (number density), and the collision frequency between particles of species η and ξ , respectively. Subscripts i , e , and n denote ions, electrons, and neutrals, all the different ions having been lumped together into one ion species and likewise all the different neutrals into one neutral species,

with composition taken into account only when determining the mean mass density ρ_η . The set of equations is completed by Ampère's and Faraday's laws

$$\mu_0 \mathbf{j} = \nabla \times \mathbf{B}, \quad \frac{\partial \mathbf{B}}{\partial t} = -\nabla \times \mathbf{E}. \quad (4)$$

[20] Note that ν_{ni} (neutral-ion collision frequency) and ν_{in} (ion-neutral collision frequency) are different quantities, related by momentum conservation in collisions which implies $\rho_n \nu_{ni} = \rho_i \nu_{in}$. To evaluate the collision frequency, we use the formulas given by *De Pontieu et al.* [2001], assuming that ions are protons and neutrals are hydrogen, and that the ions, electrons, and neutrals are in thermal equilibrium, $\nu_{in} = 7.4 \times 10^{-11} N_n T^{1/2}$, $\nu_{ni} = 7.4 \times 10^{-11} N_e T^{1/2}$, $\nu_{en} = 1.95 \times 10^{-10} N_n T^{1/2}$, and $\nu_{ei} = 3.76 N_e T^{-3/2} \ln \Lambda$, where N_n and N_e are the number densities of the neutrals and the electrons, respectively, in cm^{-3} ; the temperature T is in $^\circ\text{K}$, and $\ln \Lambda$ is the Coulomb logarithm. The collision frequencies are shown in Figure 1b. (At the present level of model development, using collision frequencies from different generally accepted references would not produce appreciable differences in the result).

[21] It is convenient to introduce also the total mass density $\rho_t = \rho_n + \rho_i = \rho_n (1 + \alpha)$ where $\alpha = \rho_i / \rho_n$; the ionization fraction $N_e / (N_e + N_n) = \rho_i / \rho_t = \alpha / (1 + \alpha)$. We have assumed that $m_i \nu_{in} \gg m_e \nu_{en}$, that the ions are singly charged, and that charge quasi-neutrality holds in the plasma, or $N_e = N_i$. Since we consider horizontal flows only, the gravitational acceleration has been omitted. For simplicity, we have neglected all other forces, in particular all the kinetic-tensor terms (flow and pressure gradients).

[22] The three terms in (1) after the electric field term are the advective ($\mathbf{V} \times \mathbf{B}$) term, the Hall term, and the resistive term, respectively. The primary use of (1) is in combination with Faraday's law (4) to obtain the time evolution of the magnetic field from $\Delta \times \mathbf{E}$. An order-of-magnitude analysis of (1), using (2) and (3) to evaluate $\mathbf{j} \times \mathbf{B}$, gives the following ratios between the terms, for variations at frequency ω :

$$\begin{aligned} \text{resistive/Hall} &= \nu_e / \Omega_e, \text{ where } \nu_e = \nu_{ei} + \nu_{en} \\ \text{Hall/advective} &= \omega / \alpha \Omega_i \text{ if } \omega \ll \nu_{ni} (\Omega_i \text{ is the ion gyrofrequency}) \\ &= \omega / \Omega_i \text{ if } \omega \gg \nu_{ni} \\ \text{resistive/advective} &= \omega \nu_e / \alpha \Omega_e \Omega_i. \end{aligned}$$

[23] If the ratio (resistive/Hall) $\ll 1$, the magnetic field is frozen to the bulk flow of the electrons, independently the ion flow and of the value of (Hall/advective). If (resistive/advective) $\ll 1$, the magnetic field is frozen to the bulk flow of the plasma as a whole; for frequencies and length scales of interest here, this condition holds throughout the entire solar atmosphere as well as in the photosphere and below. With the parameters given in Figure 1 and, in the worst case, for ω of order of 10^4 Hz, the ratios (resistive/advective) and (Hall/advective) are of the order of 10^{-2} and 10^{-4} , respectively, at the photosphere, and the former decreases rapidly with increasing altitude.

[24] We apply equations (1)–(4) to a vertically stratified and horizontally uniform, locally one-dimensional system,

with a vertical background magnetic field (of magnitude B_0 , large in comparison with the perturbed magnetic field). No vertical flow or current is considered. We assume that horizontal plasma bulk flows, oscillating at a spectrum of frequencies ω , are imposed at the lower boundary $z = 0$. For frequencies well below the neutral-ion collision frequency, $\omega \ll \nu_{ni}$, the waves propagate with $V_{At} = B/(\rho_t \mu_0)^{1/2}$, the Alfvén velocity based on the total density [see *Song et al.*, 2005, equation (31)]. Due to the nondispersive propagation in this frequency range, the perturbations will preserve their shapes as they propagate upward, although their energy flux may decrease when damping is significant. For frequencies above V_{At}/h , where h is the scale height of the chromosphere, the wavelength may be treated as small in comparison to h . Given that the observed frequency is peaked around 3.3 mHz, this approximation may hold well for weak background magnetic field (but may need to be modified for a strong magnetic field, in a future study). Under this approximation, the waves can be treated as propagating in a locally uniform medium. Horizontal flow disturbances then propagate upward along the background magnetic field as Alfvén waves.

[25] The velocity difference between the plasma and the neutrals is governed by equation (3) and for oscillatory motion is given by

$$\mathbf{V} - \mathbf{U} = -\frac{i\omega}{\nu_{ni}} \frac{1}{1 - i\omega/\nu_{ni}} \mathbf{V}. \quad (5)$$

When $\omega \ll \nu_{ni}$, the plasma and the neutrals move in synchronism with a small phase shift [*Song et al.*, 2005] and therefore the total mass density ρ_t appears in all the relations. In particular, in this low-frequency limit, inserting (5) into the plasma momentum equation (2) reduces the latter to the simple form

$$\rho_t \frac{\partial \mathbf{V}}{\partial t} = \mathbf{j} \times \mathbf{B}$$

i.e., the plasma velocity behaves as if it were subject to the Lorentz force only, the effect of collisions appearing as the replacement of the plasma density by the total density. For low frequencies $\omega \ll \alpha \Omega_i \Omega_e / \nu_e$ (negligible resistive/advective ratio, as discussed above) and $\omega \ll \alpha \Omega_i$ (negligible Hall/advective ratio), the generalized Ohm's law (1) is reduced to the simple MHD approximation $0 = \mathbf{E} + \mathbf{V} \times \mathbf{B}$. Combining these two simple equations with Ampère's and Faraday's laws (4) implies that the magnetic field perturbation $\delta \mathbf{B}$ is related to the velocity perturbation \mathbf{V} by $\delta \mathbf{B} = \pm(\rho_t \mu_0)^{1/2} \mathbf{V}$; this is the same as the familiar Walén relation in a fully ionized magnetized plasma but with the total density instead of the plasma density.

3.2. Heating Rate

[26] Energy dissipation through processes involving plasma-neutral bulk flow differences can be represented by the total heating rate for the entire medium [*Vasyliūnas and Song*, 2005]

$$q = \mathbf{j} \cdot (\mathbf{E} + \mathbf{V} \times \mathbf{B}) + \nu_{in} \rho_i |\mathbf{V} - \mathbf{U}|^2. \quad (6)$$

The first term on the right is the Ohmic (Joule) heating, associated with the last term in (1), which imparts heat to the plasma only, in the first instance; the second term is heating directly by plasma-neutral collisional friction, which imparts heat approximately equally to both media [*Vasyliūnas and Song*, 2005]. With a high collision rate, heat is subsequently redistributed to maintain an approximately equal temperature of both media.

[27] Taking the dot product of \mathbf{j} with the generalized Ohm's law (1) shows immediately that the Ohmic or Joule heating term in (6) is proportional to \mathbf{j}^2 . The current density can be related to the velocity difference from (2) and (5),

$$\mathbf{j} \times \mathbf{B} = \rho_n \nu_{ni} (\mathbf{V} - \mathbf{U}) \left[1 + \alpha - \frac{i\omega}{\nu_{ni}} \alpha \right], \quad (7)$$

from which it follows that (with no vertical velocity or current) the current is proportional to the velocity difference. The entire heating rate (6) is therefore proportional to the square of the velocity difference. We are interested in the value averaged over the oscillations, which for a product of two complex quantities aA is equal to $(1/2)\text{Re}(aA^*)$ and only the real part contributes to the average. From equations (1), (5), and (7), the heating rate is then given (see derivation in Appendix A) by

$$\langle q \rangle = \frac{\rho_t \omega^2 \langle V^2 \rangle}{\nu_{ni} (1 + \alpha) (1 + \omega^2 / \nu_{ni}^2)} \left\{ 1 + \kappa \left[(1 + \alpha)^2 + (\omega \alpha / \nu_{ni})^2 \right] \right\} \quad (8)$$

where $\kappa = \nu_e \nu_{in} / \Omega_e \Omega_i$, with $\langle V^2 \rangle$ the mean square value of the (fluctuating) plasma velocity. The term with the coefficient κ is the Joule heating contribution.

[28] It is of interest to consider the dependence of the heating rate $\langle q \rangle$ on frequency, degree of ionization (parameter α), and magnetic field strength. For this purpose it is convenient to introduce a collision frequency based on the total number density (ions plus neutrals), $\nu_t \equiv \nu_{in} + \nu_{ni}$; then $\nu_{in} = \nu_t / (1 + \alpha)$, $\nu_{ni} = \nu_t \alpha / (1 + \alpha)$, and equation (8) may be rewritten as

$$\langle q \rangle = \frac{\rho_t \omega^2 \langle V^2 \rangle}{\nu_t \alpha \left[1 + (1 + 1/\alpha)^2 \omega^2 / \nu_t^2 \right]} \left[1 + \kappa^* (1 + \alpha) (1 + \omega^2 / \nu_t^2) \right] \quad (9)$$

where $\kappa^* = \kappa (1 + \alpha) = \nu_e \nu_t / \Omega_e \Omega_i$. In the frequency range (I)

$$\omega \ll \nu_t \alpha / (1 + \alpha) = \nu_{ni} \quad (10)$$

(or equivalently the ionization range $\alpha \gg \omega(\nu_t - \omega)$ with $\omega < \nu_t$), the heating rate varies as ω^2 :

$$\langle q \rangle = \frac{\rho_t \omega^2 \langle V^2 \rangle}{\nu_t \alpha} [1 + \kappa^* (1 + \alpha)]. \quad (11)$$

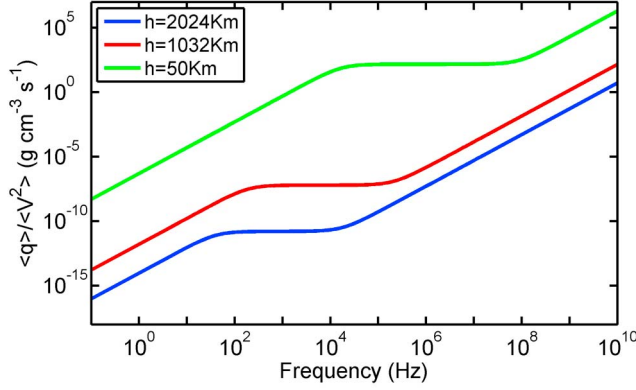


Figure 3. Heating rate divided by mean square velocity fluctuation, as function of frequency. Ionization parameters at different altitudes: $\alpha = 1.97 \times 10^{-4}$, 9.5×10^{-3} , 1.49 at 50 km, 1032 km, and 2024 km, respectively.

In the frequency range (II) $\nu_{ni} \ll \omega \ll \nu_t$ (ionization range $\alpha \ll \omega/(\nu_t - \omega)$),

$$\langle q \rangle = \frac{\rho_t \nu_t \langle V^2 \rangle \alpha}{(1 + \alpha)^2} [1 + \kappa^*(1 + \alpha)] \approx \rho_t \nu_t \langle V^2 \rangle \alpha (1 + \kappa^*) \quad (12)$$

is nearly independent of ω , and in the frequency range (III) $\omega \gg \nu_t$,

$$\langle q \rangle = \frac{\rho_t \omega^2 \langle V^2 \rangle}{\nu_t} \frac{\alpha \kappa^*}{1 + \alpha} \quad (13)$$

varies again as ω^2 . Figure 3 shows the ratio $\langle q \rangle / \langle V^2 \rangle$ as function of frequency over a very wide range, for several altitudes (having different values of α), illustrating how the heating rate varies as ω^2 at low and at high frequencies and is nearly constant in between.

[29] The above results are generally valid for a variety of different astrophysical and space settings. In the solar chromospheric heating discussion, only the frequency range (I) needs to be considered, since condition (10), $\omega \ll \nu_{ni}$, the quasi-steady state discussed in section 2.2, is amply satisfied in all regions of interest. Accordingly, we adopt equation (11) as the expression for the heating rate in the rest of this paper. The heating rate is largest at low ionization, decreases with increasing α , and in the limit of full ionization ($\alpha \rightarrow \infty$) reaches a small but nonzero value that contains Joule heating only (provided the electron collision frequency is not zero); collisional heating depends critically on the presence of both neutral and ionized constituents and thus vanishes at full ionization, but Joule heating can still be sustained by the contribution to \mathbf{j}^2 of the time derivative term in the momentum equation (2), albeit at a level smaller by a factor $1/\alpha$ than that resulting from the plasma-neutral velocity difference in the case of partial ionization.

[30] The strength of the background magnetic field plays a role primarily in determining the ratio of Joule heating to collisional heating, since κ is proportional to $1/B^2$. Joule heating can thus become dominant in regions of relatively weak magnetic field. Figure 1b shows the values of κ as a function of altitude for $B = 50\text{G}$. In this case, Joule heating

is dominant below 600 km. The heating does not, however, diverge in the limit of vanishing background field, despite what equation (8) might seem to indicate, for two reasons. First, nonlinear effects become important and constrain the heating rate when the background magnetic field is so weak that the Alfvén velocity becomes smaller than the velocity perturbation at the lower boundary; this implies, by the Walén relation, that the perturbed magnetic field is no longer small compared to the background, contrary to what we assumed in calculating \mathbf{j} from equation (7). Second, when the magnetic field is weaker still, a non-MHD regime is reached, since the ratio (resistive/advective) in the generalized Ohm’s law, discussed in section 3.1, is also proportional to $1/B^2$ and in fact equals $\kappa \omega / \nu_{ni}$. In this limit (generally not encountered in the solar atmosphere), the coupling of the magnetic field to the plasma flow, such as that described in Figure 2, breaks down; only non-magnetic (acoustic) mechanisms remain which, as discussed in the introduction, have not been able to account for the observed heating.

3.3. Altitude Dependence of Damping/Heating

[31] The amplitude of the wave was treated as constant with altitude by *De Pontieu et al.* [2001]. However, as noted earlier, for strongly damped waves the amplitude of the waves is not independent of altitude. We have found a simple way to remove this Born approximation and to determine the altitude variation of $\langle V^2 \rangle$, by invoking Poynting’s theorem:

$$\frac{\partial W}{\partial t} + \nabla \cdot \mathbf{S} = -(\mathbf{E} \cdot \mathbf{j}), \quad (14)$$

where $W = \epsilon_0 E^2/2 + B^2/2\mu_0$ is the electromagnetic energy density and $\mathbf{S} = \mathbf{E} \times \mathbf{B}/\mu_0$ is the Poynting vector. Averaged over the oscillations, $\partial W/\partial t$ is zero and \mathbf{S} has only an upward component S_z , which can be evaluated by using the Walén relationship between $\delta \mathbf{B}$ and \mathbf{V} to obtain $S_z = \rho_t V_{At} \langle V^2 \rangle$; the heating rate (11) can then be written as

$$\langle q \rangle = \frac{\omega^2 H}{\nu_{ni} V_{At} (1 + \alpha)} S_z \quad (15)$$

where $H \equiv [1 + \kappa(1 + \alpha)^2]$. The essential step in our method is the realization that in the present case (but not in general [Song et al., 2009]) $\langle q \rangle = \langle \mathbf{E} \cdot \mathbf{j} \rangle$ (see derivation in Appendix B). It follows that $\nabla \cdot \mathbf{S} = -\langle q \rangle$, which together with (15) implies (in one dimension)

$$\frac{1}{S_z} \frac{\partial S_z}{\partial z} = -\frac{\langle q \rangle}{S_z} = -\frac{\omega^2 H}{\nu_{ni} V_{At} (1 + \alpha)}; \quad (16)$$

the right-hand side is a function independent of $\langle V^2 \rangle$, allowing the spatial variation of S_z and hence of the wave amplitude to be obtained by simple integration. The method can obviously be generalized to any situation where the energy flux is carried by waves propagating predominantly in one direction (which may be variable in space). For a Poynting vector parallel to an inhomogeneous magnetic field, the left-hand side of (16) can be generalized to $(d/dl) \log(S_{\parallel}/B)$ where (d/dl) is the derivative along the field line (in this study we assume a constant magnetic field, for simplicity).

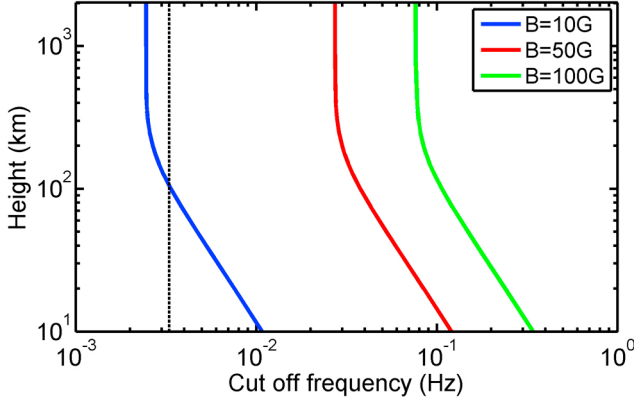


Figure 4. The upper cutoff frequency $\omega_1/2\pi$ given by equation (18) for $B = 10\text{G}$, 50G , and 100G . The vertical dashed line indicates the peak frequency of the observed waves (around 3.3 mHz).

[32] Integrating equation (16) with respect to z for a given frequency ω yields

$$S_z(z, \omega) = S_0(\omega) \exp(-\omega^2/\omega_1^2), \quad (17)$$

where $S_z(z, \omega)$ and $S_0(\omega)$ are the upward components of the time-averaged Poynting vector per unit frequency at altitude z and at the lower boundary $z = 0$, respectively, and ω_1 is defined by

$$\frac{1}{\omega_1^2(z)} \equiv \int_0^z \frac{H dz'}{V_{At} \nu_{ni} (1 + \alpha)}. \quad (18)$$

Altitude profiles of ω_1 are shown in Figure 4 for three different values of the magnetic field strength, $B = 10\text{ G}$, 50 G , and 100G . Note that ω_1 always decreases with increasing altitude, rapidly at lower altitudes but slowly above 400 km . At the lower boundary ($z = 0$) ω_1 is nominally infinite, but this simply means that the Poynting vector given by (17) correctly reproduces the assumed boundary value (see section 3.4 for further discussion). At high altitudes, as the medium becomes fully ionized ($\alpha \rightarrow \infty$), ω_1 varies very slowly and for all practical purposes approaches a finite limiting value ω_{lim} which depends strongly on the magnetic field strength: 2.5 mHz , 27 mHz , and 76 mHz for $B = 10\text{ G}$, 50 G , and 100G , respectively. Waves with frequencies below this limiting value are observable above the corona; waves with higher frequencies are strongly damped when they reach altitudes above which $\omega_1 \ll \omega$. The chromosphere thus behaves as a low-pass filter for waves, with upper cutoff frequency ω_1 locally or ω_{lim} for the entire chromosphere. One should not assume that the power and the spectrum observed at or above the corona are the same as those in the photosphere, as sometimes done in previous weakly damped Alfvén wave models. (Note that “strong” damping in this context means relative to spatial scale, not necessarily relative to wavelength; the damping distance of these waves is in fact much greater than their wavelength, see equation (32) of Song *et al.* [2005]).

[33] With the Poynting vector given by (17), the heating rate per unit frequency as a function of both altitude and

frequency can be obtained in two equivalent ways, from (15) and (16), respectively (we now deal only with averages over the oscillations and write $\langle q \rangle$ simply as q):

$$q(z, \omega) = \frac{\omega^2 H}{\nu_{ni} V_{At} (1 + \alpha)} S_0(\omega) \exp(-\omega^2/\omega_1^2), \quad \text{or} \quad (19a)$$

$$q(z, \omega) = -\frac{\partial}{\partial z} [S_0(\omega) \exp(-\omega^2/\omega_1^2)]. \quad (19b)$$

Expression (19b) is generally more convenient for actual calculation, as it avoids some convergence and limit problems particularly at $z = 0$ for power law spectra (see more detailed discussion in section 3.4), whereas (19a) may provide more physical insight. Note that ω_1 , V_{At} and ν_{ni} are all functions of altitude, and the first two are also strong functions of the background magnetic field. The heating rate (19a) is equal to the available energy flux density (Poynting vector) at the altitude considered, multiplied by a factor equal to $-(d/dz)\omega^2/\omega_1^2$ which may be considered the heat conversion efficiency per unit distance: a direct demonstration that the fraction of the energy removed from the wave by damping is what appears as heat. This efficiency of heat generation is a strong function of altitude. For a given frequency, it tends to initially decrease rapidly with increasing altitude, as κ drops from its large value at low altitudes (see Figure 1b); once κ becomes less than unity (above $\sim 600\text{ km}$), it varies slowly, reflecting the opposing effects of increasing Alfvén speed and decreasing neutral-ion collision frequency. For the same Poynting vector at a given frequency, higher frequency waves are more efficient in generating heat; the heating rate increases approximately as ω^2 in the relevant frequency range, as discussed in section 3.2.

[34] The total heating rate Q at altitude z is obtained by integrating q over frequency:

$$Q(z) = \int_0^\infty q(z, \omega) d\omega = -\frac{d}{dz} F(z) \quad (20)$$

where

$$F(z) = \int_0^\infty S_0(\omega) \exp(-\omega^2/\omega_1^2) d\omega = \int_0^\infty S_z(z, \omega) d\omega \quad (21)$$

is the total (integrated over all frequencies) wave energy flux density at altitude z , which reduces to the source energy flux density

$$F_0 = \int_0^\infty S_0(\omega) d\omega \quad (22)$$

at the lower boundary (identified with the surface of the photosphere) $z = 0$, where $\omega_1 \rightarrow \infty$ (If z is taken at the top of the chromosphere, $\omega_1 \rightarrow \omega_{lim}$.) The total power that goes into generating heat in the chromosphere, given by the integral of Q over altitude z , is simply

$$\int_0^z Q(z') dz' = F_0 - F(z). \quad (23)$$

3.4. Evaluation for a Source of Power Law Frequency Spectrum

[35] To evaluate the heating rate, one has to know the spectrum of the perturbations at the lower boundary. In an illustrative specific model, discussed further in section 5.1, we assume that at the surface of the photosphere the perturbation peak frequency is ω_0 and that the spectrum above ω_0 can be described by a power law with slope $-n$ ($n < -1$) [see, e.g., *Kolmogorov*, 1941; *Batchelor*, 1953], extending from ω_0 nominally to infinity; for simplicity, we neglect all power in the spectrum below ω_0 . With the normalization (22), the Poynting vector then is at the lower boundary $z = 0$

$$S_0(\omega) = \begin{cases} (n-1) \frac{F_0}{\omega_0} \left(\frac{\omega}{\omega_0}\right)^{-n} & \omega \geq \omega_0 \\ 0 & \omega < \omega_0 \end{cases} \quad (24)$$

and at a given altitude z

$$S_z(z, \omega) = \begin{cases} (n-1) \frac{F_0}{\omega_0} \left(\frac{\omega}{\omega_0}\right)^{-n} \exp(-\omega^2/\omega_1^2) & \omega \geq \omega_0 \\ 0 & \omega < \omega_0 \end{cases} \quad (25)$$

Since $n > 1$, the contribution of the high frequencies to the wave energy flux decreases and becomes insignificant well below ν_{ni} , ensuring the validity of the approximation $\omega \ll \nu_{ni}$. A similar initial spectrum has been employed in previous models [e.g., *Tsiklauri and Nakariakov*, 2001]. Our results are not sensitive to the exact shape of the initial spectrum, provided it is normalized to the appropriate total flux.

[36] There are two factors that determine the wave spectrum (25): a power law drop at high frequencies, the slope of which is imposed by the spectrum at the lower boundary (possibly controlled by a cascading process as discussed in section 5.1), and an exponential drop due to the frequency dependence of the damping. Because ω_1 decreases with altitude, so does the Poynting vector at a fixed frequency.

rate Q at altitude z can be calculated in two equivalent ways: either taking the frequency integration of (19a), which gives

$$Q(z) = F_0 \frac{n-1}{2} \frac{\omega_1^2 H}{\nu_{ni} V_{At} (1+\alpha)} \left(\frac{\omega_0}{\omega_1}\right)^{n-1} \Gamma\left(\frac{3-n}{2}, \frac{\omega_0^2}{\omega_1^2}\right) \quad (27a)$$

or, invoking (20), corresponding to the frequency integration of (19b), by differentiating $F(z)$ given by (26). A simpler version in this latter method obtained by combining (27a) with (26) yields

$$Q(z) = \frac{n-1}{2} \frac{\omega_1^2 H}{\nu_{ni} V_{At} (1+\alpha)} [F_0 \exp(-\omega_0^2/\omega_1^2) - F(z)]. \quad (27b)$$

The first method is the more convenient one in most cases. However, there potentially exists a singular point. At $z = 0$, where $1/\omega_1 = 0$ by definition, the *incomplete* Γ -function reduces to the Γ -function, which is constant for a given n , (see i.e., equation (C6)). When the power law index $n \leq 3$, $Q(0)$ appears to go to infinity. This singularity is in general removable, and in the worst case it will produce only a small loss in precision (see Appendix D for further discussion). The second expression, on the other hand, may be useful in regions of weak damping where the variation of the energy flux density may be so slow as to render the evaluation of the derivative inaccurate.

[38] Since the *incomplete* Γ -function is defined for $a > 0$, or $n > 3$, (26) and (27a) are valid only for $n < 3$. When $n > 3$, subtle manipulations are needed to avoid a negative index a , (see Appendix C for details). For weakly damping, or $\omega_0^2 \ll \omega_1^2$, the small-argument expansion of $\Gamma(a, x)$ for $x \ll 1$ gives to lowest order in ω_0/ω_1 (see Appendix C) from (26)

$$F(z) \approx \begin{cases} F_0 \left[1 - \left(\frac{\omega_0}{\omega_1}\right)^{n-1} \Gamma\left(\frac{3-n}{2}\right) + \frac{n-1}{3-n} \left(\frac{\omega_0}{\omega_1}\right)^2 \right] & \text{for } n < 3 \\ F_0 \left[1 - \frac{n-1}{n-3} \left(\frac{\omega_0}{\omega_1}\right)^2 \right] & \text{for } n > 3 \end{cases} \quad (28)$$

and from (27a)

$$Q(z) \approx \begin{cases} F_0 \frac{n-1}{2} \frac{\omega_1^2 H}{\nu_{ni} V_{At} (1+\alpha)} \left[\left(\frac{\omega_0}{\omega_1}\right)^{n-1} \Gamma\left(\frac{3-n}{2}\right) - \frac{2}{3-n} \left(\frac{\omega_0}{\omega_1}\right)^2 \right] & \text{for } n < 3 \\ F_0 \frac{n-1}{n-3} \frac{\omega_1^2 H}{\nu_{ni} V_{At} (1+\alpha)} \frac{1}{2} \left(\frac{\omega_0}{\omega_1}\right)^2 & \text{for } n > 3 \end{cases} \quad (29)$$

[37] The total flux (21) at a given altitude is now (details of the frequency integrations are given in Appendix C)

$$F(z) = \int_{\omega_0}^{\infty} S_z(z, \omega) d\omega \\ = F_0 \left[\exp(-\omega_0^2/\omega_1^2) - \left(\frac{\omega_0}{\omega_1}\right)^{n-1} \Gamma\left(\frac{3-n}{2}, \frac{\omega_0^2}{\omega_1^2}\right) \right] \quad (26)$$

where $\Gamma(a, x) = \int_x^{\infty} e^{-y} y^{a-1} dy$ is the *incomplete* Γ -function [see, e.g., *Abramowitz and Stegun*, 1965]. The total heating

(see Appendix C for discussion of the mathematically singular case $n = 3$). If $\omega_0^2 \ll \omega_{lim}^2$, a significant amount of low-frequency wave power is propagating into the upper chromosphere. In the opposite case to strong damping, $\omega_0^2 \gg \omega_1^2$, the large-argument expansion of $\Gamma(a, x)$ for $x \gg 1$ gives

$$F(z) \cong F_0 \left[\frac{n-1}{2} \left(\frac{\omega_1}{\omega_0}\right)^2 \exp(-\omega_0^2/\omega_1^2) \right]; \quad (30)$$

i.e., negligible wave power remains, as expected.

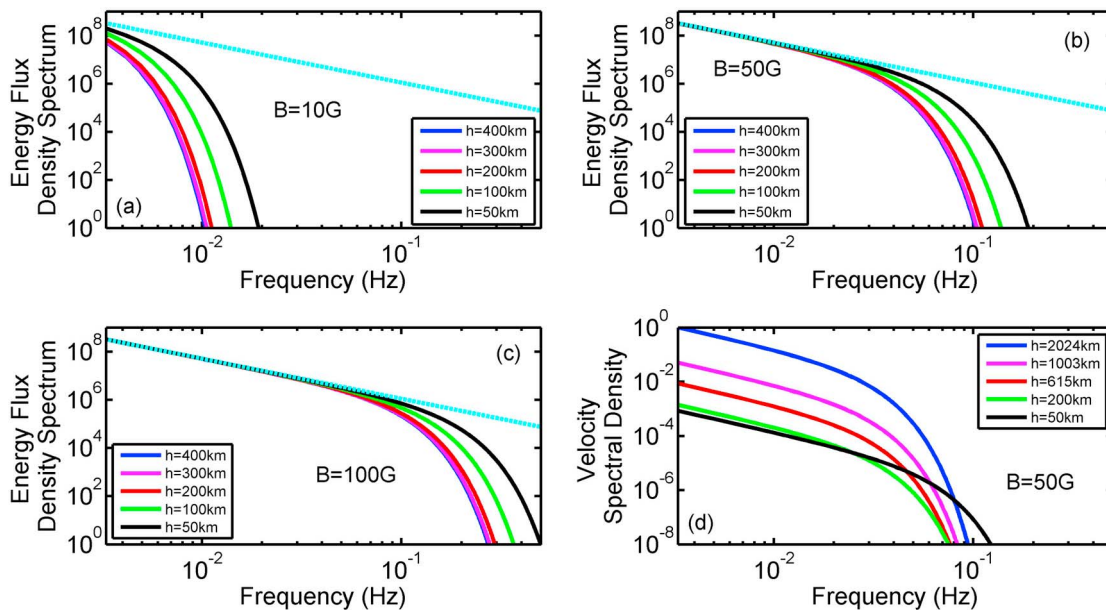


Figure 5. Spectra of the model energy flux density from equation (25) with $F_0 = 10^7 \text{ erg cm}^{-2} \text{ s}^{-1}$ and $n = 5/3$, at different altitudes, for (a) $B = 10\text{G}$, (b) $B = 50\text{G}$, and (c) $B = 100\text{G}$, respectively. Dashed lines represent the unmodified power law spectrum. The chromospheric parameters used in the calculation are from Figure 1. (d) The corresponding spectral density of the velocity for $B = 50\text{G}$, normalized to the spectrum at 2024 km.

[39] The different behavior for power law exponent larger or smaller than 3, see (29), reflects the fact that for $n < 3$ (which includes the physically interesting case $n = 5/3$), heating proportional to ω^2 diverges at the high-frequency limit, and what keeps the total heating rate Q finite is only the exponential cut-off in (25) at all $z \neq 0$ (avoidance of the implied singularity near $z = 0$ is an important advantage of the first method for calculating Q). For $n > 3$, Q is always finite and the exponential cut-off is not essential.

4. Application to the Solar Chromosphere and Comparison With Observations

[40] To apply our 1-dimensional model to the solar chromosphere requires that the scales of spatial variation be much longer in the two horizontal dimensions than in the vertical. The scale in the vertical direction is less than 2000 km and, as we will show next, the most significant heating in our model occurs below 1000 km. As the perturbations considered in our model are associated with the supergranules, which have horizontal scales of 3×10^4 km, the 1-dimensional approximation is applicable.

4.1. Change of Spectrum With Altitude

[41] For illustration purposes, we assume that on the surface of the Sun, the spectrum follows the power law given by equation (24); as parameter values we adopt total energy flux density $F_0 \sim 10^7 \text{ erg cm}^{-2} \text{ s}^{-1}$ [De Pontieu et al., 2001] and frequency of peak power $\omega_0/2\pi = 1/300 \text{ s}$, corresponding to the 5 min oscillation peak in observations [e.g., Cranmer et al., 2007]. Figures 5a, 5b, and 5c show the frequency spectra of the Poynting vector (25) in units of energy

flux density per unit frequency (erg cm^{-2}), at various altitudes, for $n = 5/3$ and the background magnetic field $B = 10\text{G}$, 50G , and 100G , respectively. Also shown is the unmodified power law spectrum (24). The effective upper cutoff frequency ω_1 corresponds to the onset of a significant (on the logarithmic scale) deviation of the spectrum downward from the power law. As the altitude increases, the power in the high frequencies is damped more strongly; also, the weaker the background magnetic field, the stronger the damping. In the case of $B = 10\text{G}$, all the spectra lie below the power law, indicating that the limiting upper cutoff frequency $\omega_{\text{lim}}/2\pi$ lies below the peak frequency $\omega_0/2\pi$. If B is much less than 10G , the wave power above the chromosphere is predicted by (30) to be more than one order of magnitude weaker than that in the photosphere. For $B = 50\text{G}$ and 100G , by contrast, ω_{lim} lies well above ω_0 , and a range of negligibly weak damping is evident at the lower frequencies, in which waves can propagate into the upper chromosphere.

[42] If waves that have propagated up to the corona or above and can be observed there are taken as indicative of the energy flux density within the chromosphere (neglecting the damping), the Alfvén wave damping calculated from the observed spectrum does not provide much heating, a reason why previous weakly damped Alfvén-wave models had difficulty to produce adequate heating. Even worse, because more wave power is expected to propagate into the upper chromosphere when the magnetic field magnitude is larger, a misleading conclusion may be drawn that heating is enhanced by a stronger magnetic field, whereas the real situation is just the opposite: heating is enhanced by a weaker magnetic field. If the magnetic field magnitude is

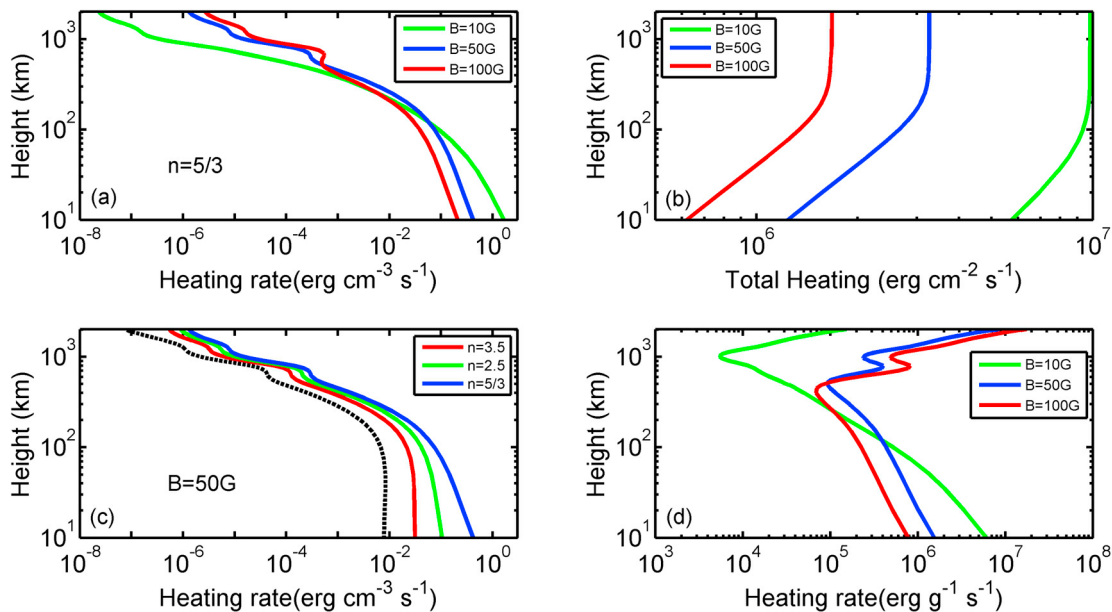


Figure 6. (a) The total heating rate (in $\text{erg cm}^{-3} \text{s}^{-1}$), assuming $F_0 = 10^7 \text{ erg cm}^{-2} \text{s}^{-1}$, as functions of altitude for $n = 5/3$, for $B = 10\text{G}$, 50G , and 100G . The chromospheric parameters are those used in Figures 1 and 4. (b) The height integrated heat for the heating rates shown in Figure 6a. (c) The total heating rate for $B = 50\text{G}$ and $n = 3.5$, 2.5 , and $5/3$, in the same format as Figure 6a. The corresponding heating rate from equation (13) of *De Pontieu et al. [2001]* for $1/f = 5 \text{ min}$ (calculated using the same solar parameters) is shown by the dashed line, for comparison. (d) The heating rate divided by the mass density (in $\text{erg g}^{-1} \text{s}^{-1}$), for the same parameters as in Figure 6a.

sufficiently small to make the limiting upper cutoff frequency much less than the peak frequency of the source, all the waves are expected to be heavily damped in the chromosphere. The physical reason for the stronger damping in a weaker magnetic field can be easily understood: when gyromotion is more dominant relative to collision effects, less heat is produced. (In the extremely weak field limit, as the background field goes to zero, limitations imposed by nonlinear and non-MHD effects have been discussed in section 3.2).

[43] Velocity fluctuation rather than the Poynting vector is the more commonly observed quantity. Figure 5d shows the frequency spectra of mean square velocity, equal to $S_z/(\rho_t V_{At})$; the curves (plotted as relative values normalized to unity at 3.3 mHz and altitude 2024 km) correspond to the Poynting-vector spectra shown in Figure 5b. Within the undamped lower-frequency range of the spectrum, the mean square velocity increases with increasing altitude, in contrast to the energy flux which is independent of altitude in this frequency range. This discrepancy is simply the result of the density decrease with altitude in the solar atmosphere; an observed altitude variation of velocity fluctuation amplitudes is not, therefore, by itself a reliable indicator of where the source of the perturbations is located. The undamped portion of Figure 5d is roughly consistent with the observed frequency and altitude dependence reported by *Reardon et al. [2008, Figure 2]*: the power spectrum of the velocity increases about two orders of magnitude from 200 km to 1000 km (the frequency range of the observations lies below the upper cutoff frequencies of our model and does not

include any portion of the spectrum where strong damping is expected). The observed quantity in work by *Reardon et al. [2008]*, however, is the vertical component of the velocity, presumably the result of predominantly acoustical wave modes. The comparison with our present model of horizontal velocities from Alfvén modes is thus of at most qualitative significance.

[44] For $F_0 \sim 10^7 \text{ erg cm}^{-2} \text{s}^{-1}$, the total peak spectral density for the horizontal velocity components at the photosphere is $0.36 \text{ (km/s)}^2 \text{ mHz}^{-1}$, corresponding to 2.7 km/s of the averaged velocity amplitude, for $n = 5/3$. The velocity is subsonic, consistent with the observed perturbation velocities [*Avrett and Loeser, 2008; Jess et al., 2009*], and should occur more often than the strong wave event reported by *De Pontieu et al. [2007]*.

4.2. Total Heating Rate and Energy Budget

[45] Figure 6a shows the altitude profile of the total heating rate per unit volume (in $\text{erg cm}^{-3} \text{s}^{-1}$) for an assumed source spectrum with the same parameters as in section 4.1, calculated from (27a), plotted as functions of altitude for $n = 5/3$ and $B = 10\text{G}$, 50G , and 100G . Note that since the point $z = 0$ is not included in this calculation, the singularity at the lower boundary has no effect. The heating rate depends strongly on the background magnetic field and weaker fields produce more heat at lower altitudes. This can be easily understood from the dependence of the upper cutoff frequency on magnetic field strength (discussed in section 3.3 and shown in Figure 4) and should not depend in a qualitatively major way on the exact form of the source

spectrum. At high altitudes, the heating rate is much reduced and its dependence on the magnetic field is reversed, stronger fields producing relatively more heat. This is simply because less energy loss to heating below means more energy flux left available above. The total heating rate Q is 10^{-1} erg cm $^{-3}$ s $^{-1}$ or more at the lower chromosphere and 10^{-2} erg cm $^{-3}$ s $^{-1}$ at the middle and upper chromosphere, consistent with the empirical estimates of what is needed to sustain the radiative losses [Withbroe and Noyes, 1977; Vernazza et al., 1981].

[46] Figure 6b shows the altitude profile of the total heating rate per unit column area, integrated from the lower boundary up to altitude z . At the top of the chromosphere, the total integrated heating rates are 9.8, 3.3, and 1.7×10^6 erg cm $^{-2}$ s $^{-1}$ for $B = 10$ G, 50G, and 100G, respectively, adequate for the required heating in the chromosphere [Withbroe and Noyes, 1977]. In general, if the background magnetic field is below 10G, most of the wave power is damped to heat the solar atmosphere; if it is above 100G, most of the waves are only weakly damped. It is thus not surprising that Alfvén waves are only observed sparsely, and then primarily when the background magnetic field is strong [e.g., Ulrich, 1996; De Pontieu et al., 2007].

[47] To illustrate the effect of varying the power law index, Figure 6c shows the heating rates per unit volume for $n = 5/3, 2.5,$ and $3.5,$ with $B = 50$ G and with the same values of F_0 and ω_0 as before. The primary effect of a steeper index (less wave power at higher frequencies) is to reduce the heating rate everywhere, as expected from the ω^2 dependence discussed in section 3.2. The reduction is more pronounced at lower altitudes, but the altitude profile as a whole is not greatly changed. We have calculated the total integrated heating rates: 3.3, 1.1, and 0.5×10^6 erg cm $^{-2}$ s $^{-1}$ for $n = 5/3, 2.5,$ and $3.5,$ respectively; the value in the limit $n \rightarrow \infty$ is 0.37×10^6 erg cm $^{-2}$ s $^{-1}$. Most of the reduction occurs around $n = 3,$ the index above which the heating rate no longer diverges at high frequencies in absence of the exponential cutoff.

[48] For comparison, the heating rate from Alfvén wave damping derived by De Pontieu et al. [2001] is shown by the dashed line in Figure 6c. Their model treated only a single frequency and thus corresponds to $n \rightarrow \infty$ in our model; the dashed line in Figure 6c looks indeed like the asymptotic limit for large n . Since De Pontieu et al. [2001] employed the Born approximation and thus did not include strong damping, their model is self-consistent only in the parameter range $\omega_0^2 \ll \omega_{\text{lim}}^2$, which for 3.3 mHz (5-min period) holds for magnetic fields stronger than 50G. As seen in Figure 6c, their model provides only 2% of the heating in comparison to ours—not enough to account for the observations.

[49] Figure 6d shows the heating rate per unit mass, Q/ρ_t a quantity widely used in coronal heating studies. This is the heating per particle and can be large either because the heating rate is high (e.g., below 400 km) or because the density is low (e.g., above 1000 km). The reversed dependence on magnetic field strength between low and high altitudes, noted for the total heating rates in Figure 6a, is here particularly pronounced. This feature of our model, that at higher altitudes the heating per unit mass is greater for stronger field, may be related to some recent observations [e.g., De Pontieu et al., 2011], such as spicules which are

structures with strong magnetic field and high temperature extending from the upper chromosphere into the corona.

5. Discussion

5.1. Source of the Waves

[50] The basic physics of our model does not depend on a specific shape of the frequency spectrum, which determines only the specific numerical values, e.g., the heating rate and the height of the maximum heating. A power law spectrum is a convenient approximation which simplifies the mathematical treatment and supplies an analytical solution.

[51] A power law spectrum can be generated by turbulent flow below the photosphere, or below the lower boundary of our model. In well-developed turbulence, a cascading process transfers energy from longer-wavelength to shorter-wavelength perturbations to form a power law spectrum, starting from the intrinsic frequency of the disturbance source, which we identify with the observed 5-min oscillations. In a spectrum, this frequency appears as the peak frequency; there is little wave power below it, and the cascading processes transfer energy to higher frequencies with a decreasing power density. We can thus take the peak frequency, ω_0 , as the lower cutoff frequency of the wave energy, and we assume that the spectrum above ω_0 can be described by a power law with slope $-n$ [see, e.g., Kolmogorov, 1941; Batchelor, 1953]. Observations of the perturbation spectra [e.g., Ulrich, 1996; Fossum and Carlsson, 2005; Reardon et al., 2008] show in general a peak frequency near 1/300s, for 5-min period oscillations, and small power in both higher and lower frequencies. In our model, higher frequency waves are more efficient in generating heating and, even if they may carry only a small fraction of the total wave power, may still play an important (if not dominant) role in solar atmospheric heating.

[52] The perturbation power at the photosphere will in general be different in vertical and horizontal directions. The physical process described by our model does not rely on an anisotropy in the perturbations although only perturbations perpendicular to the background magnetic field contribute, and in our presently assumed simplified geometry they are horizontal. Observations have nonetheless indicated that horizontal perturbations are dominant in the low chromosphere [e.g., Avrett and Loeser, 2008]. Vertical perturbations are important in some other mechanisms (e.g., shock heating) which may complement our model at high altitudes.

5.2. Possible Nonlinear Wave Effects

[53] So far we have assumed that the perturbation spectrum is produced by cascading below the photosphere and propagates into the chromosphere, where the higher frequencies are absorbed. The cascading may, however, continue to occur at higher altitudes, transferring energy from lower to higher frequencies also in the chromosphere. Ideally, the cascading process does not generate more total wave power, and power gained at higher frequencies is that lost at lower frequencies. However, since (as we have shown) high frequency waves are more efficient in generating heat, this secondary cascading can lead

to more heating and to a higher total heating rate. The size of the effect depends on the cascading time compared with the upward wave propagation time. If the former is much shorter than the latter, the cascading process in the chromosphere will contribute significantly to the chromospheric heating, otherwise not. Beyond the chromosphere in the corona, on the other hand, the propagation time can be very long and the secondary cascading may be important.

6. Conclusions

[54] We have developed a model for heating the solar atmosphere by strong damping of Alfvén waves injected from the photosphere and below. The damping mechanism is interaction between plasma and the neutral particles in the weakly ionized medium, specifically, frictional dissipation by ion-neutral collisions together with Joule heating (the result of electron collisions). The theory includes self-consistently the collisions among electrons, ions, and neutrals, the interaction between charged particles and the electromagnetic field, and the reduction of the wave energy flux by the damping. Although so far we have treated only the geometrically simple case of one-dimensional stratified atmosphere, the model already predicts (with reasonable parameter values and without invoking anomalous processes) heating rates consistent with what is inferred from observations. Furthermore, in contrast to most previous models, the predicted spatial distribution places the bulk of the heating in the lower chromosphere, the place where it is required by the observations.

[55] Two essential elements of our treatment are the use of Poynting's theorem to determine self-consistently the altitude profile of the wave energy flux and the inclusion of a broad frequency spectrum (whereas previous models of heating by damping of Alfvén waves mostly treated a single frequency and assumed an altitude-independent wave power). A broad spectrum is particularly important because the rate of heating by the mechanism under discussion increases as ω^2 , and hence the high frequency portion of the spectrum contributes to the heating more than its proportionate share of the wave power. The exact form of the wave spectrum determines quantitatively the heating rate but does not affect the applicability of the mechanism. For a power law initial spectrum in the photosphere, the energy flux as a function of frequency and height is given in (25).

[56] Since our present simplified model is one-dimensional, the background magnetic field can only be described as an average over a large area. Within this limitation, the model predicts that, for a given wave energy flux in the photosphere, heating is stronger in the weaker-field regions. This result may appear to many to be counter-intuitive, but it has a firm physical basis: Joule heating is enhanced when electron gyromotion becomes less important relative to collisions.

[57] The damping of the high-frequency waves with increasing altitude (an indispensable ingredient of the heating mechanism) implies that they are filtered out by the chromosphere and cannot be observed above the transition region. To verify this effect observationally,

there are two opposing requirements: significant wave power, requiring weak damping and a stronger magnetic field, and lower upper cutoff frequency, requiring a weaker field. These may be difficult to meet with currently available techniques.

[58] In view of observations showing that the chromosphere is highly dynamic in time with many fine structures [e.g., *Jess et al.*, 2009; *De Pontieu et al.*, 2007] and given the long history of unsuccessful attempts to model the quasi-steady state chromospheric heating, it has been argued [*Carlsson and Stein*, 1997] that the solar atmosphere may not be in equilibrium and there does not exist an equilibrium state of the system. Without taking sides in the debate over whether the quasi-steady state is a useful concept to study solar atmospheric heating [e.g., *Carlsson*, 2007; *Martínez-Sykora et al.*, 2008; *Vecchio et al.*, 2009], we note that the quasi-steady state is useful to describe the time average of a system which may or may not be in equilibrium. Our zeroth-order or quasi-steady state model (which does not describe explosive processes and is, moreover, so far highly simplified geometrically) has shown that the solar atmosphere heating problem can be understood, at least in orders of magnitude, with simple concept and processes if the analysis is conducted self-consistently.

[59] We have focused on the lower altitudes of the solar atmosphere, below 1000 km. Other mechanisms, possibly involving compressional or acoustic modes, may be acting at higher altitudes. Furthermore, turbulence [e.g., *Hollweg*, 1986; *Heyvaerts and Priest*, 1983; *Inverarity and Priest*, 1995; *Matthaeus et al.*, 1999] and reconnection [e.g., *Sturrock and Uchida*, 1981; *Parker*, 1988] may also play some roles in the heating process. All these could contribute to the overall final understanding of the solar atmosphere heating problem; we claim no exclusivity for our mechanism. Nevertheless, our model appears to provide the bulk of the required heating at the right place, and this suggests that the underlying physical mechanism is likely to be a key constituent of a successful theory. Detailed comparison with observations will be made when the model is developed to a more realistic stage.

Appendix A: Heating Rate

[60] From (1), the Ohmic heating rate is,

$$\mathbf{j}^* \cdot (\mathbf{E} + \mathbf{V} \times \mathbf{B}) = m_e \nu_e |\mathbf{j}|^2 / N_e e^2. \quad (\text{A1})$$

From (7)

$$|\mathbf{j}|^2 = \mathbf{j} \cdot \mathbf{j}^* = (\rho_n \nu_{ni} / B)^2 \left[(1 + \alpha)^2 + (\alpha \omega / \nu_{ni})^2 \right] |\mathbf{V} - \mathbf{U}|^2. \quad (\text{A2})$$

Combining (A2) with (A1) gives the Ohmic heating as

$$\mathbf{j}^* \cdot (\mathbf{E} + \mathbf{V} \times \mathbf{B}) = \frac{\nu_e \nu_{in}}{\Omega_e \Omega_i} \left[(1 + \alpha)^2 + (\alpha \omega / \nu_{ni})^2 \right] \rho_n \nu_{ni} |\mathbf{V} - \mathbf{U}|^2. \quad (\text{A3})$$

The conversion from the velocity difference to the perturbation velocity, from (5):

$$|\mathbf{V} - \mathbf{U}|^2 = \frac{1}{1 + \omega^2/\nu_{ni}^2} \left(\frac{\omega}{\nu_{ni}} \right)^2 |\mathbf{V}|^2. \quad (\text{A4})$$

The total heating rate (damping rate) is obtained by adding together Ohmic heating and collisional friction heating:

$$\begin{aligned} \langle q \rangle &= \mathbf{j}^* \cdot \mathbf{V} \times \mathbf{B} + \nu_{in} \rho_i |\mathbf{V} - \mathbf{U}|^2 \\ &= \left\{ 1 + \frac{\nu_e \nu_{in}}{\Omega_e \Omega_i} \left[(1 + \alpha)^2 + (\alpha \omega / \nu_{ni})^2 \right] \right\} \rho_n \nu_{ni} \langle (\mathbf{V} - \mathbf{U})^2 \rangle \\ &= \left\{ 1 + \frac{\nu_e \nu_{in}}{\Omega_e \Omega_i} \left[(1 + \alpha)^2 + (\alpha \omega / \nu_{ni})^2 \right] \right\} \frac{\omega^2}{\nu_{ni} (1 + \omega^2 / \nu_{ni}^2)} \rho_n \langle \mathbf{V}^2 \rangle. \end{aligned} \quad (\text{A5})$$

Appendix B: Relation Between the Heating Rate and $\mathbf{E} \cdot \mathbf{j}$

[61] Note that $\mathbf{E} \cdot \mathbf{j}$ depends on frame of reference while q does not; in general, $\mathbf{E} \cdot \mathbf{j}$ includes heating and possible work done. The two are equal in a specific frame of reference under certain conditions. In our treatment, \mathbf{E} and \mathbf{S} are both defined in the frame of reference of the local solar atmosphere, essentially at rest relative to the Sun. In our frame of reference, from (6) we have

$$q - \mathbf{E} \cdot \mathbf{j} = \mathbf{j} \cdot \mathbf{V} \times \mathbf{B} + \nu_{in} \rho_i |\mathbf{V} - \mathbf{U}|^2;$$

use the plasma momentum equation (2) to eliminate $\mathbf{j} \times \mathbf{B}$

$$q - \mathbf{E} \cdot \mathbf{j} = -\rho_i \frac{\partial \mathbf{V}}{\partial t} \cdot \mathbf{V} + \nu_{ni} \rho_n \mathbf{U} \cdot (\mathbf{U} - \mathbf{V}),$$

and the neutral momentum equation (3) to eliminate $\mathbf{U} - \mathbf{V}$, obtaining

$$q - \mathbf{E} \cdot \mathbf{j} = -\frac{\partial}{\partial t} \left(\frac{1}{2} \rho_i V^2 + \frac{1}{2} \rho_n U^2 \right).$$

The right-hand side vanishes when averaged over the oscillations, thus $\langle q \rangle = \langle \mathbf{E} \cdot \mathbf{j} \rangle$, QED. When other forces are present, this simple relationship may not hold.

Appendix C: Derivations of Flux and Total Heating Rate for Power Law Spectrum

[62] Derivation of the flux, equation (26): substituting (25) into (22) obtains

$$F(z) = \int_{\omega_0}^{\infty} d\omega (n-1) \frac{F_0}{\omega_0} \left(\frac{\omega}{\omega_0} \right)^{-n} e^{-\omega^2/\omega_1^2}. \quad (\text{C1})$$

Set $u \equiv \omega^2/\omega_1^2$

$$\frac{F}{F_0} = \frac{n-1}{2} \left(\frac{\omega_0}{\omega_1} \right)^{n-1} \int_{\omega_0^2/\omega_1^2}^{\infty} du u^{-\frac{n+1}{2}} e^{-u}. \quad (\text{C2})$$

Integration by parts (integrate $u^{-(n+1)/2}$ first) yields

$$\begin{aligned} \frac{F}{F_0} &= -\left(\frac{\omega_0}{\omega_1} \right)^{n-1} \left[u^{\frac{1-n}{2}} e^{-u} \Big|_{\omega_0^2/\omega_1^2}^{\infty} + \int_{\omega_0^2/\omega_1^2}^{\infty} du u^{\frac{3-n}{2}-1} e^{-u} \right] \\ &= e^{-\omega_0^2/\omega_1^2} - \left(\frac{\omega_0}{\omega_1} \right)^{n-1} \Gamma\left(\frac{3-n}{2}, \frac{\omega_0^2}{\omega_1^2} \right) \end{aligned} \quad (\text{C3})$$

which is (26).

[63] Derivation of the total heating rate, equation (27a): substituting (25) into (15), the first expression of (20) becomes

$$Q = \int_{\omega_0}^{\infty} q(z, \omega) d\omega = \int_{\omega_0}^{\infty} d\omega F_0 \frac{(n-1)\omega_0 H}{\nu_{ni} V_{At} (1+\alpha)} \left(\frac{\omega}{\omega_0} \right)^{2-n} e^{-\omega^2/\omega_1^2}. \quad (\text{C4})$$

Set $u \equiv \omega^2/\omega_1^2$

$$\begin{aligned} Q &= \frac{q_0 \omega_1}{2} \left(\frac{\omega_0}{\omega_1} \right)^{n-1} \int_{\omega_0^2/\omega_1^2}^{\infty} du u^{\frac{3-n}{2}-1} e^{-u} \\ &= \frac{q_0 \omega_1}{2} \left(\frac{\omega_0}{\omega_1} \right)^{n-1} \Gamma\left(\frac{3-n}{2}, \frac{\omega_0^2}{\omega_1^2} \right) \end{aligned} \quad (\text{C5})$$

which is (27a); $q_0 \equiv F_0 \frac{(n-1)\omega_1 H}{\nu_{ni} V_{At} (1+\alpha)}$.

[64] The *incomplete* Γ -function is reduced to the Γ -function for small argument $x \ll 1$

$$\Gamma(a, x) \approx \Gamma(a) - \frac{x^a}{a} \left(1 - \frac{x}{a+1} + \dots \right) \quad (\text{C6})$$

(valid only for $a > 0$), and for large argument $x \gg 1$

$$\Gamma(a, x) \approx x^{a-1} e^{-x} \left[1 + \frac{a-1}{x} + \frac{(a-1)(a-2)}{x^2} + \dots \right] \quad (\text{C7})$$

which can be used to simplify the heating rates for parameter ranges of $\omega_0 \ll \omega_1$ and $\omega_0 \gg \omega_1$, respectively.

[65] The *incomplete* Γ -function is defined for $a > 0$, or $n > 3$; or (C5) is valid for $n < 3$. When $n > 3$, one must then continue the integration by parts in equation (C3), or equivalently invoke the recurrence relation

$$\Gamma(a+1, x) = a\Gamma(a, x) + x^a e^{-x},$$

repeatedly until one reaches a positive index a ; then the expansion (C6) can be applied. For example, for $3 < n < 5$

$$\begin{aligned} \frac{F}{F_0} &= -\left(\frac{\omega_0}{\omega_1}\right)^{n-1} \left[u^{\frac{1-n}{2}} e^{-u} \Big|_{\omega_0^2/\omega_1^2}^{\infty} + \frac{2}{3-n} u^{\frac{3-n}{2}} e^{-u} \Big|_{\omega_0^2/\omega_1^2}^{\infty} + \frac{2}{3-n} \int_{\omega_0^2/\omega_1^2}^{\infty} du u^{\frac{5-n}{2}-1} e^{-u} \right] \\ &= e^{-\omega_0^2/\omega_1^2} \left[1 - \frac{2}{n-3} \left(\frac{\omega_0}{\omega_1}\right)^2 \right] + \left(\frac{\omega_0}{\omega_1}\right)^{n-1} \frac{2}{n-3} \Gamma\left(\frac{5-n}{2}, \frac{\omega_0^2}{\omega_1^2}\right). \end{aligned} \quad (C8)$$

For $5 < n < 7$

$$\begin{aligned} \frac{F}{F_0} &= -\left(\frac{\omega_0}{\omega_1}\right)^{n-1} \left[u^{\frac{1-n}{2}} e^{-u} \Big|_{\omega_0^2/\omega_1^2}^{\infty} + \frac{2}{3-n} u^{\frac{3-n}{2}} e^{-u} \Big|_{\omega_0^2/\omega_1^2}^{\infty} + \right. \\ &\quad \left. + \frac{2}{3-n} \frac{2}{5-n} \left(u^{\frac{5-n}{2}} e^{-u} \Big|_{\omega_0^2/\omega_1^2}^{\infty} + \int_{\omega_0^2/\omega_1^2}^{\infty} du u^{\frac{7-n}{2}-1} e^{-u} \right) \right] \\ &= e^{-\omega_0^2/\omega_1^2} \left[1 - \frac{2}{n-3} \left(\frac{\omega_0}{\omega_1}\right)^2 + \frac{4}{(n-3)(n-5)} \left(\frac{\omega_0}{\omega_1}\right)^4 \right] - \left(\frac{\omega_0}{\omega_1}\right)^{n-1} \frac{4}{(n-3)(n-5)} \Gamma\left(\frac{7-n}{2}, \frac{\omega_0^2}{\omega_1^2}\right) \end{aligned} \quad (C9)$$

and so on. It is apparent that for $n \rightarrow \infty$, i.e., for effectively a single frequency ω_0 , $F/F_0 \rightarrow \exp -(\omega_0^2/\omega_1^2)$.

[66] When n is large but not infinite, since the lowest-order term is $(\omega_0/\omega_1)^2$, the flux ratio can be approximated by expanding the exponential function:

$$\frac{F}{F_0} \approx \left[1 - \left(\frac{\omega_0}{\omega_1}\right)^2 \right] \left[1 - \frac{2}{n-3} \left(\frac{\omega_0}{\omega_1}\right)^2 \right] \cong \left[1 - \frac{n-1}{n-3} \left(\frac{\omega_0}{\omega_1}\right)^2 \right]. \quad (C10)$$

Equations (C7) through (C10) as well as the $n \gg 3$ expressions in equations (28) and (29) of the main text apply only if n is well above 3. The case $n = 3$ can be treated by noting that the *incomplete* Γ -function with zero index a may be expressed as the exponential integral:

$$\Gamma(0, x) = \int_x^{\infty} e^{-t} t^{-1} dt = E_1(x) \quad (C11)$$

which has the expansions ($\gamma = 0.5772157\dots$ Euler's constant)

$$\begin{aligned} E_1(x) &= -\log x - \gamma + x - \frac{x^2}{2 \times 2!} + \dots & x \ll 1 \\ &= e^{-x} \left[\frac{1}{x} - \frac{1}{x^2} + \dots \right] & x \gg 1 \end{aligned}$$

Appendix D: Remarks on Convergence and Limits

[67] To calculate the total flux, $F(z)$, or total heating rate, $Q(z)$, one integrates (17) or (19a) over the frequency, respectively. As $1/\omega_1 = 0$ at $z = 0$, by definition, for the heating rate $Q(z)$ the exponential factor in (19a) becomes 1 and the convergence of the frequency integration is determined by the frequency dependence of the Poynting flux

$S_0(\omega)$. When the power law index $n \leq 3$, the integral for the heating rate Q with its factor of ω^2 does not converge at the

high-frequency limit. This singularity becomes more obvious in (27a). On the other hand, this singularity does not occur in the total flux integration $F(z)$ because the flux is well defined at the lower boundary by (20).

[68] Below we show that the singularity for $Q(z)$ at $z = 0$ (or $1/\omega_1 = 0$), when $n \leq 3$, is in general removable.

[69] Assume first the upper limit of the integration to be ω' and then let ω' go to infinity; i.e., take the source spectrum as

$$S_0(\omega) = (n-1) \frac{F_0}{\omega_0} \left(\frac{\omega_0}{\omega}\right)^n \text{ for } \omega_0 < \omega < \omega', = 0 \text{ otherwise} \quad (D1)$$

More precisely, F_0 should be replaced by $F_0(1 - (\omega_0/\omega')^{n-1})^{-1}$ in all the equations below. Then the total heating rate is the integral from ω_0 to ω' , equal to the integral from ω_0 to ∞ minus that from ω' to ∞ . Equation (27a) then becomes

$$Q = \{\dots\} \omega_1^2 \left(\frac{\omega_0}{\omega_1}\right)^{n-1} \left[\Gamma\left(\frac{3-n}{2}, \frac{\omega_0^2}{\omega_1^2}\right) - \Gamma\left(\frac{3-n}{2}, \frac{\omega'^2}{\omega_1^2}\right) \right] \quad (D2)$$

where $\{\dots\} = F_0 \frac{(n-1)H}{2\nu_m V_{At}(1+\alpha)}$. If $\omega' \gg \omega_1$, the second Γ -function becomes negligible (see large-argument expansion, equation (C7)) and we recover the original equation (27a).

[70] If $\omega_1 \gg \omega'$ and $\omega_1 \ll \omega_0$ (as near $z = 0$ where $\omega_1 \rightarrow \infty$), the small-argument expansion (equation (C6)) gives for the term in brackets $\frac{2}{3-n} \left[\left(\frac{\omega'}{\omega_1}\right)^{3-n} - \left(\frac{\omega_0}{\omega_1}\right)^{3-n} \right]$ and thus

$$Q \approx \{\dots\} \frac{2\omega_0^2}{3-n} \left[\left(\frac{\omega'}{\omega_0}\right)^{3-n} - 1 \right] \quad (D3)$$

This is independent of ω_1 , hence there is no problem as $\omega_1 \rightarrow \infty$.

[71] **Acknowledgments.** The authors thank E.N. Parker for illuminating comments, B. De Pontieu for useful discussions, and Y. Wang for preparing the figures. This work was supported by the National Science Foundation under grant AGS-0903777.

[72] Philippa Browning thanks the reviewers for their assistance in evaluating this paper.

References

- Abramowitz, M., and I. A. Stegun (Eds.) (1965), *Handbook of Mathematical Functions*, pp. 260, Dover, New York.
- Aschwanden, M. (2005), *Physics of the Solar Corona: An Introduction With Problems and Solutions*, Springer, New York.
- Athay, R. G. (1976), *The Solar Chromosphere and Corona: Quiet Sun*, D. Reidel, Dordrecht, Netherlands.
- Avrett, E. H., and R. Loeser (2008), Models of the solar chromosphere and transition region from SUMER and HRTS observatory: Formation of the extreme-ultraviolet spectrum of hydrogen, carbon, and oxygen, *Astrophys. J. Suppl. Ser.*, 175, 229, doi:10.1086/523671.
- Banerjee, D., D. Pérez-Suárez, and J. G. Doyle (2009), Signatures of Alfvén waves in the polar coronal holes as seen by EIS/Hinode, *Astron. Astrophys.*, 501, L15, doi:10.1051/0004-6361/200912242.
- Batchelor, G. K. (1953), *The Theory of Homogeneous Turbulence*, Cambridge Univ. Press, New York.
- Böhm-Vitense, E. (1984), Chromospheres, transition regions, and coronas, *Science*, 223, 777, doi:10.1126/science.223.4638.777.
- Carlsson, M. (2007), Modeling the solar chromosphere, in *The Physics of Chromospheric Plasmas*, *Astron. Soc. Pac. Conf. Ser.*, vol. 368, edited by P. Heinzel, I. Dorotović, and R. J. Rutten, p. 49, Astron. Soc. of the Pac., San Francisco, Calif.
- Carlsson, M., and R. F. Stein (1997), Formation of calcium H and K grain, *Astrophys. J.*, 481, 500, doi:10.1086/304043.
- Cranmer, S. R., A. A. van Ballegoijen, and R. J. Edgar (2007), Self-consistent coronal heating and solar wind acceleration from anisotropic magnetohydrodynamic turbulence, *Astrophys. J. Suppl. Ser.*, 171, 520, doi:10.1086/518001.
- De Pontieu, B., P. C. H. Martens, and H. S. Hudson (2001), Chromospheric damping of Alfvén waves, *Astrophys. J.*, 558, 859, doi:10.1086/322408.
- De Pontieu, B., et al. (2007), Chromospheric Alfvén waves strong enough to power the solar wind, *Science*, 318, 1574, doi:10.1126/science.1151747.
- De Pontieu, B., S. W. McIntosh, M. Carlsson, V. H. Hansteen, T. D. Tarbell, P. Boerner, J. Martínez-Sykora, C. J. Schrijver, and A. M. Title (2011), The origins of hot plasma in the solar corona, *Science*, 331, 55, doi:10.1126/science.1197738.
- Erdélyi, R., and V. Fedun (2007), Are there Alfvén waves in the solar atmosphere?, *Science*, 318, 1572, doi:10.1126/science.1153006.
- Fossum, A., and M. Carlsson (2005), High-frequency acoustic waves are not sufficient to heat the solar chromosphere, *Nature*, 435, 919, doi:10.1038/nature03695.
- Goodman, M. L. (2004), On the creation of the chromospheres of solar type stars, *Astron. Astrophys.*, 424, 691, doi:10.1051/0004-6361:20040310.
- Haerendel, G. (1992), Weakly damped Alfvén waves as driver of solar chromospheric spicules, *Nature*, 360, 241.
- Heyvaerts, J., and E. R. Priest (1983), Coronal heating by phase-mixed shear Alfvén waves, *Astron. Astrophys.*, 117, 220.
- Hollweg, J. V. (1985), Energy and momentum transport by waves in the solar atmosphere, in *Advances in Space Plasma Physics*, edited by B. Buti, pp. 77, World Sci., Singapore.
- Hollweg, J. V. (1986), Transition region, corona, and solar wind in coronal holes, *J. Geophys. Res.*, 91, 4111, doi:10.1029/JA091iA04p04111.
- Hollweg, J. V., and P. A. Isenberg (2002), Generation of the fast solar wind: A review with emphasis on the resonant cyclotron interaction, *J. Geophys. Res.*, 107(A7), 1147, doi:10.1029/2001JA000270.
- Inverarity, G. W., and E. R. Priest (1995), Turbulence coronal heating: II. Twisted flux tube, *Astron. Astrophys.*, 296, 395.
- Jess, D. B., M. Mathioudakis, R. Erdélyi, P. J. Crockett, F. P. Keenan, and D. J. Christian (2009), Alfvén waves in the lower solar atmosphere, *Science*, 323, 1582, doi:10.1126/science.1168680.
- Khodachenko, M. L., T. D. Arber, H. O. Rucker, and A. Hanslmeier (2004), Collisional and viscous damping of MHD wave in partially ionized plasmas of the solar atmosphere, *Astron. Astrophys.*, 422, 1073, doi:10.1051/0004-6361:20034207.
- Kolmogorov, A. N. (1941), The local structure of turbulence in incompressible viscous fluid for very large Reynolds number, *Dokl. Akad. Nauk SSSR*, 30, 301.
- Leake, J. E., T. D. Arber, and M. L. Khodachenko (2005), Collisional dissipation of Alfvén waves in a partial ionized solar atmosphere, *Astron. Astrophys.*, 442, 1091, doi:10.1051/0004-6361:20053427.
- Martínez-Sykora, J., V. Hansteen, and M. Carlsson (2008), Twisted flux tube emergence from the convection zone to the corona, *Astrophys. J.*, 679, 871, doi:10.1086/587028.
- Matthaeus, W. H., G. P. Zank, S. Oughton, D. J. Mullan, and P. Dmitruk (1999), Coronal heating by magnetohydrodynamic turbulence driven by reflected low-frequency waves, *Astrophys. J.*, 523, L93, doi:10.1086/312259.
- Narain, U., and P. Ulmschneider (1990), Chromospheric and coronal heating mechanisms, *Space Sci. Rev.*, 54, 377.
- Narain, U., and P. Ulmschneider (1996), Chromospheric and coronal heating mechanisms II, *Space Sci. Rev.*, 75, 453, doi:10.1007/BF00833341.
- Osterbrock, D. E. (1961), The heating of the solar chromosphere, plages, and corona by magnetohydrodynamic waves, *Astrophys. J.*, 134, 347, doi:10.1086/147165.
- Parker, E. N. (1965), Dynamical theory of the solar wind, *Space Sci. Rev.*, 4, 666, doi:10.1007/BF00216273.
- Parker, E. N. (1988), Nanoflares and the solar X-ray corona, *Astrophys. J.*, 330, 474, doi:10.1086/166485.
- Parker, E. N. (1991), Heating solar coronal holes, *Astrophys. J.*, 372, 719, doi:10.1086/170015.
- Piddington, J. H. (1956), Solar atmospheric heating by hydromagnetic waves, *Mon. Not. R. Astron. Soc.*, 116, 314.
- Priest, E. R. (2000), *Solar Magneto-hydrodynamics*, *Geophys. Astrophys. Monogr.*, D. Reidel, Dordrecht, Netherlands.
- Reardon, K. P., F. Lepreti, V. Carbone, and A. Vecchio (2008), Evidence of shock-driven turbulence in the solar chromosphere, *Astrophys. J.*, 683, L207–L210, doi:10.1086/591790.
- Soler, R., R. Oliver, and J. L. Ballester (2011), Spatial damping of propagating kink waves in prominence threads, *Astrophys. J.*, 726, 102.
- Song, P., V. M. Vasyliūnas, and L. Ma (2005), Solar wind-magnetosphere-ionosphere coupling: Neutral atmosphere effects on signal propagation, *J. Geophys. Res.*, 110, A09309, doi:10.1029/2005JA011139.
- Song, P., V. M. Vasyliūnas, and X.-Z. Zhou (2009), Magnetosphere-ionosphere/thermosphere coupling: Self-consistent solutions for a one-dimensional stratified ionosphere in three-fluid theory, *J. Geophys. Res.*, 114, A08213, doi:10.1029/2008JA013629.
- Sturrock, P. A., and Y. Uchida (1981), Coronal heating by stochastic magnetic pumping, *Astrophys. J.*, 246, 331, doi:10.1086/158926.
- Terradas, J., M. Goossens, and G. Verth (2010), Selective spatial damping of propagating kink waves due to resonant absorption, *Astron. Astrophys.*, 524, A23, doi:10.1051/0004-6361/201014845.
- Tsiklauri, D., and V. M. Nakariakov (2001), Wide-spectrum slow magnetoacoustic waves in coronal loops, *Astron. Astrophys.*, 379, 1106, doi:10.1051/0004-6361:20011378.
- Ulmschneider, P. (2001), Chromospheric heating mechanisms, in *Encyclopedia of Astronomy and Astrophysics*, edited by P. Murdin, Nature Pub. Group, Bristol, U. K.
- Ulrich, R. K. (1996), Observations of magnetohydrodynamic oscillations in the solar atmosphere with properties of Alfvén waves, *Astrophys. J.*, 465, 436, doi:10.1086/177431.
- Van de Hulst, H. C. (1953), The chromosphere and the corona, in *The Sun*, edited by G. P. Kuiper, chap. 5, p. 257, Univ. of Chicago Press, Chicago, Ill.
- Van Doorselaere, T., V. M. Nakariakov, and E. Verwichte (2008), Detection of waves in the solar corona: Kink or Alfvén?, *Astrophys. J.*, 676, L73, doi:10.1086/587029.
- Vasheghani Farahani, S., V. M. Nakariakov, T. Van Doorselaere, and E. Verwichte (2011), Nonlinear long-wavelength torsional Alfvén waves, *Astron. Astrophys.*, 526, A80, doi:10.1051/0004-6361/201016063.
- Vasyliūnas, V. M., and P. Song (2005), Meaning of ionospheric Joule heating, *J. Geophys. Res.*, 110, A02301, doi:10.1029/2004JA010615.
- Vecchio, A., G. Cauzzi, and K. P. Reardon (2009), The solar chromosphere at high resolution with IBIS II. Acoustic shocks in the quiet internetwork and the role of magnetic fields, *Astron. Astrophys.*, 494, 269, doi:10.1051/0004-6361:200810694.
- Vernazza, J. E., E. H. Avrett, and R. Loeser (1981), Structure of the solar chromosphere. III — Models of the EUV brightness components of the quiet-sun, *Astrophys. J. Suppl. Ser.*, 45, 635, doi:10.1086/190731.

Verth, G., J. Terradas, and M. Goossens (2010), Observational evidence of resonantly damped propagating kink waves in the solar corona, *Astrophys. J.*, 718, L102, doi:10.1088/2041-8205/718/2/L102.

Withbroe, G. L., and R. W. Noyes (1977), Mass and energy flow in the solar chromosphere and corona, *Annu. Rev. Astron. Astrophys.*, 15, 363, doi:10.1146/annurev.aa.15.090177.002051.

P. Song, Department of Environmental, Earth and Atmospheric Sciences, University of Massachusetts Lowell, Lowell, MA 01854, USA. (paul_song@uml.edu)

V. M. Vasyliūnas, Max-Planck-Institut für Sonnensystemforschung, D-37191 Katlenburg-Lindau, Germany.